Dynamic Aeroelastic Analysis Using Reduced-Order Modeling with Error Estimation

Brandon M. Lowe * and David W. Zingg †
Institute for Aerospace Studies, University of Toronto,
4925 Dufferin St, Toronto, Ontario, M3H 5T6, Canada

This paper presents a methodology for dynamic aeroelastic analysis of aircraft based on model order reduction with error estimation. A projection-based model order reduction approach is used to create an aerodynamic reduced-order model (ROM) which is coupled to a structural model to create an aeroelastic ROM. The governing aerodynamic equations are the linearized semi-discrete Euler equations. Flutter analysis is conducted by analyzing the eigenvalues of the aeroelastic ROM. A dual-weighted residual-based error estimator is presented which approximates the error in the eigenvalues obtained from the reduced eigenproblem relative to the eigenvalues from the high-dimensional aeroelastic model. The error estimator thus allows for the construction of aeroelastic ROMs with select eigenvalues that satisfy a user-prescribed accuracy. The aerodynamic ROM is constructed using approximate high-dimensional aeroelastic eigenvectors computed using the two-sided Jacobi-Davidson algorithm. Dynamic aeroelastic analyses are presented for a two degree of freedom structural model and for the AGARD 445.6 wing test case. The error estimator is shown to have good agreement with the exact error. For the test cases presented in this work, the cost of computing the flutter point at a given Mach number is equivalent to the cost of approximately 4 to 5 steady nonlinear flow evaluations of the high-dimensional Euler equations.

I. Introduction

In recent years, a strong emphasis has been placed on the need for increased aircraft fuel efficiency. Efficient designs can be conceived with the aid of aerodynamic shape optimization and multidisciplinary optimization tools based on high-fidelity computational fluid dynamics (CFD) [1]. However, the resulting unconventional aircraft are typically designed to fly at transonic Mach numbers, where a dip in the flutter boundary typically occurs due to shock formation and motion.

Linear aerodynamic methods (such as the doublet lattice method) have been widely used for flutter predictions in the past due to their low computational cost. However, these methods fail to model nonlinear flow features accurately in the transonic regime [2]. This lack of accuracy has led to overly conservative aircraft designs and hence reduced fuel efficiency [3]. Alternatively, time-dependent high-dimensional CFD simulations present a means to model aerodynamics accurately for dynamic aeroelastic analysis. However, due to the unsteady nature of the problem, the large number of degrees of freedom, and the number of flight conditions to consider, the use of CFD for flutter predictions in a design context remains intractable. As a result, numerous CFD-based alternatives have been proposed for flutter predictions. A number of researchers have applied a Hopf point calculation method to obtain the flutter point of CFD-based aeroelastic systems [4–6]. Jacobson *et al*. [7] presented a linearized frequency-domain approach for predicting the onset of flutter. Their approach uses a p-k flutter analysis method with generalized aerodynamic forces obtained from the solutions of the linearized Reynolds-averaged Navier-Stokes (RANS) equations in the frequency domain. He *et al*. [8] have presented a time-spectral approach to solve for the flutter point of the aeroelastic equations. They simultaneously solve for flutter speed index and the flutter frequency along with the flow states at all time instances. Opgenoord *et al*. [9] have developed a low-order aerodynamic model which is calibrated using two-dimensional high-fidelity CFD simulations and uses strip theory to extend its applications to three-dimensional geometries.

A large breadth of literature has also been devoted to the application of model order reduction for flutter analysis [10–27]. These methods aim to generate reduced-order models (ROMs) which accurately capture the dynamic behavior of the high-dimensional model (HDM) in a fraction of the computational time. In the case of flutter analysis, the CFD

*PhD Candidate, University of Toronto, brandon.lowe@mail.utoronto.ca
†University of Toronto Distinguished Professor of Computational Aerodynamics and Sustainable Aviation, Director, Centre for Research in Sustainable Aviation, dwz@oddjob.utias.utoronto.ca

model constitutes the HDM. We do not provide an exhaustive survey of the field, but here we describe a few notable applications of ROMs for aeroelastic analyses. Hall *et al*. [10] and Thomas *et al*. [11] were among the first to use a proper orthogonal decomposition (POD)-based ROM for aeroelastic modeling. Using the linearized Euler equations in the frequency-domain, they constructed ROMs which provide flutter boundaries with good agreement to solutions from the HDM. A few years later, Lieu *et al*. [14, 15] modeled the dynamic aeroelastic behavior of a complete aircraft configuration using a POD-based ROM constructed from the frequency-domain linearized Euler equations. Beran *et al*. [12] used a POD-based ROM to predict the onset of limit-cycle oscillations for a nonlinear panel in a two-dimensional flow. Silva *et al*. [19, 20] performed flutter predictions by constructing aerodynamic ROMs based on aerodynamic forces from high-dimensional CFD simulations using the eigensystem realization algorithm [28]. Argaman and Raveh [26] have modeled an aeroelastic system as a multi-output autoregressive process with model parameters identified using aeroelastic responses from CFD solutions. Previously, the authors of this paper have also presented a ROM-based approach for flutter predictions [27]. In this previous work, an aerodynamic ROM was constructed using a reduced basis created by applying POD to snapshots obtained by exciting the structural states during a single unsteady flow solve. The aerodynamic ROM was then coupled to the structural model, and the eigenvalues of the resulting aeroelastic ROM were analyzed to predict the onset of flutter.

All of the aforementioned ROM-based approaches are capable of predicting flutter. However, none are capable of estimating the accuracy of their flutter prediction relative to the original aeroelastic HDM. In this paper, we present a ROM-based aeroelastic analysis approach with an error estimator capable of providing a user-prescribed level of accuracy for flutter predictions relative to the aeroelastic HDM. Dynamic aeroelastic analysis is performed by analyzing the eigenvalues of the aeroelastic ROM. The dual-weighted residual (DWR) method [29] is used to provide an error estimate for the eigenvalues. The error estimator provides the user with a measure of accuracy for the approximated aeroelastic eigenvalues and also serves as an indicator to determine at which flight conditions to update the reduced basis. This leads to an automated ROM training procedure for which the user needs only to supply some parameters for initial snapshots, a range of relevant flight conditions, and the desired level of accuracy in the eigenvalues. Furthermore, an extension of the eigenvalue error estimator is presented to obtain approximate errors for the predicted flutter point. Similar to the work by Lowe and Zingg [27], we rely on the linearized semi-discrete Euler equations as our high-dimensional aerodynamic system; however the reduced basis is now constructed using approximate eigenvectors of the aeroelastic HDM obtained using the two-sided refined Jacobi-Davidson algorithm [30–32]. Our use of eigenvectors and the two-sided Jacobi-Davidson algorithm for model order reduction is similar to the work presented by Benner *et al*. [33]. However, in our work, the left eigenvectors are not used for the test basis in the construction of the ROM, but are rather used to construct a second ROM for error estimation. We also note that the methodology presented herein is not limited to the use of the linearized Euler equations, and can be extended to the linearized RANS equations.

It has been shown that the DWR method provides effective error estimation for aerodynamic problems [34] as well as eigenvalue problems [35]. The DWR method requires the solution to a dual (or adjoint) problem in a subspace not spanned by the reduced basis used to create the aeroelastic ROM. We approximate dual solutions with a second aerodynamic ROM created using a reduced basis trained on dual solutions. As will be discussed in Section IV, the dual solution to the aeroelastic eigenproblem is in fact the left eigenpair of the system. Thus, we denote the aeroelastic ROM used for the main aeroelastic analysis as the *primal ROM*, and the aeroelastic ROM used for the error analysis as the *dual ROM*.

The remainder of this paper is divided into the following sections. In Section II, we present the high-dimensional equations used to model aeroelastic behavior, including the structural and aerodynamic models. Section III describes the model order reduction approach used to create the primal aeroelastic ROM. In Section IV, we give an overview of the error estimator derivation, and describe the procedure to create the dual aeroelastic ROM. Section V presents our methodology for training the primal and dual reduced bases for accurate flutter predictions. Section VI gives the approach for obtaining the flutter point once the ROM has been sufficiently trained, and also presents the extension of the error estimator to compute the error in the predicted flutter point. Lastly, Section VII contains the results obtained using the methodology derived in this paper.

II. High-Dimensional Semi-discrete Aeroelastic Model

This section presents the high-dimensional semi-discrete equations used to model dynamic aeroelastic behavior. An overview of the structural model is first presented. Subsequently, the linearized semi-discrete Euler equations are derived and used to form the aerodynamic model. Finally, the structural and aerodynamic models are coupled to form the high-dimensional monolithic aeroelastic model. For ease of presentation, certain quantities associated to the aerodynamic model are indicated with the subscript a, whereas those for the structural models are presented with the subscript s.

A. Structural Model

For dynamic aeroelastic analysis, structural states are commonly expanded into a modal series consisting of the summation of free vibration modes weighted by time-dependent generalized displacements. Neglecting contributions from damping, one may write the resulting equations of motion as follows:

$$\frac{d^2\boldsymbol{u}_{\mathrm{s,tot}}}{dt_{\mathrm{s}}^2} + \Omega_{\mathrm{s}}\boldsymbol{u}_{\mathrm{s,tot}} = \boldsymbol{f}_{\mathrm{s,tot}} \tag{1}$$

where t_{s} is the time variable for the structural model, $\boldsymbol{u}_{\mathrm{s,tot}}$ is the vector of generalized displacements, $\boldsymbol{f}_{\mathrm{s,tot}}$ is the vector of generalized forces applied to the structural grid, and Ω_{s} is a diagonal matrix of squared natural frequencies. We wish to linearize equation (1) about a steady-state solution. The relevant states are expanded as:

$$\boldsymbol{u}_{\mathrm{s,tot}} = \boldsymbol{u}_{\mathrm{s,0}} + \boldsymbol{u}_{\mathrm{s}}, \qquad \boldsymbol{u}_{\mathrm{a,tot}} = \boldsymbol{u}_{\mathrm{a,0}} + \boldsymbol{u}_{\mathrm{a}}, \tag{2}$$

where $\boldsymbol{u}_{\mathrm{a,tot}}$ is the vector of aerodynamic states, and steady-state quantities are denoted with the subscript 0. Interest lies in modeling the state fluctuations $\boldsymbol{u}_{\mathrm{s}}$ and $\boldsymbol{u}_{\mathrm{a}}$, and their impact on the fluctuations of the applied forces: $\boldsymbol{f}_{\mathrm{s}} = \boldsymbol{f}_{\mathrm{s,tot}} - \boldsymbol{f}_{\mathrm{s,0}}$.

Forces are computed on the aerodynamic grid, which does not correspond to the structural grid. Additionally, the aerodynamic equations are typically nondimensionalized and thus applied forces require a dimensionalization factor. We introduce the force scaling factor σ_{f}, the force transfer matrix T_{f}, and the displacement transfer matrix T_{d}, such that

$$\boldsymbol{f}_{\mathrm{s}} = \sigma_{\mathrm{f}} T_{\mathrm{f}} \boldsymbol{f}_{\mathrm{a}}, \qquad \boldsymbol{x}_{\mathrm{a,surf}} = T_{\mathrm{d}}\boldsymbol{u}_{\mathrm{s}}, \tag{3}$$

where $\boldsymbol{f}_{\mathrm{a}}$ is the vector of aerodynamic force fluctuations computed on the aerodynamic surface grid, and $\boldsymbol{x}_{\mathrm{a,surf}}$ is the vector of aerodynamic surface grid node coordinate fluctuations. The transfer matrices T_{f} and T_{d} may be computed in a number of ways. For complex structural geometries, popular methods include Rendall and Allen's radial basis function interpolation [36], and Brown's rigid link method [37]. For two degree of freedom structural models acting at a single point, the transfer matrix can be formed using a small angle approximation. As the applied forces are a function of both the aerodynamic and structural states, we can use the transfer matrices to exchange information between structural and aerodynamic grids. Expanding the fluctuations of the force into a Taylor series and truncating high-order terms gives,

$$\boldsymbol{f}_{\mathrm{s}} = \sigma_{\mathrm{f}} T_{\mathrm{f}} \boldsymbol{f}_{\mathrm{a}} \approx \sigma_{\mathrm{f}} T_{\mathrm{f}} \left(\frac{\partial \boldsymbol{f}_{\mathrm{a}}}{\partial \boldsymbol{x}_{\mathrm{a,surf}}} T_{\mathrm{d}} \boldsymbol{u}_{\mathrm{s}} + \frac{\partial \boldsymbol{f}_{\mathrm{a}}}{\partial \boldsymbol{u}_{\mathrm{a}}} \boldsymbol{u}_{\mathrm{a}} \right). \tag{4}$$

The linearized structural model thus becomes,

$$\frac{d^2\boldsymbol{u}_{\mathrm{s}}}{dt_{\mathrm{s}}^2} = A_{\mathrm{s}}\boldsymbol{u}_{\mathrm{s}} + C_s \boldsymbol{u}_{\mathrm{a}}, \tag{5}$$

where:

$$A_{\mathrm{s}} = \sigma_{\mathrm{f}} T_{\mathrm{f}} \frac{\partial \boldsymbol{f}_{\mathrm{a}}}{\partial \boldsymbol{x}_{\mathrm{a,surf}}} T_{\mathrm{d}} - \Omega_{\mathrm{s}}, \qquad C_s = \sigma_{\mathrm{f}} T_{\mathrm{f}} \frac{\partial \boldsymbol{f}_{\mathrm{a}}}{\partial \boldsymbol{u}_{\mathrm{a}}}.$$

B. Aerodynamic Model

The governing aerodynamic equations used for dynamic aeroelastic analysis are the linearized semi-discrete Euler equations. Before linearization, the Euler equations are discretized in space using a second-order summation-by-parts approach, and are then put into an arbitrary Lagrangian-Eulerian form. This leads to the following set of ordinary differential equations:

$$\frac{dJ^{-1}\boldsymbol{u}_{\mathrm{a,tot}}}{dt_{\mathrm{a}}} = \boldsymbol{R}_{\mathrm{a}} \left(\boldsymbol{u}_{\mathrm{a,tot}}(t_{\mathrm{a}}), \boldsymbol{x}_{\mathrm{a,vol,tot}}(t_{\mathrm{a}}), \dot{\boldsymbol{x}}_{\mathrm{a,vol,tot}}(t_{\mathrm{a}}) \right). \tag{6}$$

Here $\boldsymbol{x}_{\mathrm{a,vol,tot}}$ and $\dot{\boldsymbol{x}}_{\mathrm{a,vol,tot}}$ are the vectors of volume grid node coordinates and velocities, respectively. Additionally, t_{a} is the time variable for the aerodynamic model, $\boldsymbol{R}_{\mathrm{a}}$ is the residual vector, and J^{-1} is a diagonal matrix of inverse metric Jacobians of the transformation to curvilinear coordinates. In order to preserve a uniform flow in the presence of a deforming grid, the evolution of the J^{-1} is governed by the Geometric Conservation Law [38].

The linearized semi-discrete Euler equations are obtained by assuming the flow states, grid node coordinates, and grid node velocities can be represented as linear fluctuations about a nonlinear steady-state:

$$\boldsymbol{u}_{\mathrm{a,tot}} = \boldsymbol{u}_{\mathrm{a},0} + \boldsymbol{u}_{\mathrm{a}}, \qquad \boldsymbol{x}_{\mathrm{a,vol,tot}} = \boldsymbol{x}_{\mathrm{a,vol},0} + \boldsymbol{x}_{\mathrm{a,vol}}, \qquad \dot{\boldsymbol{x}}_{\mathrm{a,vol,tot}} = \dot{\boldsymbol{x}}_{\mathrm{a,vol}}. \tag{7}$$

Steady-state grid node velocities are assumed to be zero. The resulting linearized semi-discrete Euler equations are:

$$J_0^{-1}\frac{d\boldsymbol{u}_{\mathrm{a}}}{dt_{\mathrm{a}}} + \frac{\partial \boldsymbol{R}_{\mathrm{a}}}{\partial \boldsymbol{u}_{\mathrm{a}}}\boldsymbol{u}_{\mathrm{a}} + \frac{\partial \boldsymbol{R}_{\mathrm{a}}}{\partial \boldsymbol{x}_{\mathrm{a,vol}}}K_{\mathrm{m}}\boldsymbol{x}_{\mathrm{a,surf}} + \left(\frac{\partial}{\partial \dot{\boldsymbol{x}}_{\mathrm{a,vol}}}\left(\frac{dJ^{-1}}{dt_{\mathrm{a}}}\right)\boldsymbol{u}_{\mathrm{a},0} + \frac{\partial \boldsymbol{R}_{\mathrm{a}}}{\partial \dot{\boldsymbol{x}}_{\mathrm{a,vol}}}\right)K_{\mathrm{m}}\dot{\boldsymbol{x}}_{\mathrm{a,surf}} = \boldsymbol{0}, \tag{8}$$

where K_{m} is a linear mesh movement matrix such that:

$$\boldsymbol{x}_{\mathrm{a,vol}} = K_{\mathrm{m}}\boldsymbol{x}_{\mathrm{a,surf}}, \qquad \dot{\boldsymbol{x}}_{\mathrm{a,vol}} = K_{\mathrm{m}}\dot{\boldsymbol{x}}_{\mathrm{a,surf}}. \tag{9}$$

Here $\boldsymbol{x}_{\mathrm{a,surf}}$ and $\dot{\boldsymbol{x}}_{\mathrm{a,surf}}$ are the vectors of aerodynamic surface grid node coordinate fluctuations and velocities. For details on the derivation of the linearized Euler equations, see Lowe and Zingg [27].

The aerodynamic model is nondimensionalized in time differently than the structural model. To address this, the following time scaling factor is introduced:

$$t_{\mathrm{s}} = \sigma_{\mathrm{t}} t_{\mathrm{a}}. \tag{10}$$

Additionally, as for the force transfer discussed above, we must transfer displacements from the structural grid to the aerodynamic surface grid. We use the displacement transfer matrix T_{d} such that,

$$\boldsymbol{x}_{\mathrm{a,surf}} = T_{\mathrm{d}}\boldsymbol{u}_{\mathrm{s}}, \qquad \frac{d\boldsymbol{x}_{\mathrm{a,surf}}}{dt_{\mathrm{a}}} = \sigma_{\mathrm{t}} T_{\mathrm{d}}\frac{d\boldsymbol{u}_{\mathrm{s}}}{dt_{\mathrm{s}}}, \tag{11}$$

Introducing equations (10) and (11) into (8), the aerodynamic model is given by,

$$E_{\mathrm{a}}\frac{d\boldsymbol{u}_{\mathrm{a}}}{dt_{\mathrm{s}}} = A_{\mathrm{a}}\boldsymbol{u}_{\mathrm{a}} + B_{\mathrm{a},1}\boldsymbol{u}_{\mathrm{s}} + B_{\mathrm{a},2}\frac{d\boldsymbol{u}_{\mathrm{s}}}{dt_{\mathrm{s}}}, \tag{12}$$

where the system matrices are:

$$E_{\mathrm{a}} = \sigma_{\mathrm{t}} J_0^{-1}, \qquad A_{\mathrm{a}} = \frac{\partial \boldsymbol{R}_{\mathrm{a}}}{\partial \boldsymbol{u}_{\mathrm{a}}}, \qquad B_{\mathrm{a},1} = \frac{\partial \boldsymbol{R}_{\mathrm{a}}}{\partial \boldsymbol{x}_{\mathrm{a,vol}}}K_{\mathrm{m}}T_{\mathrm{d}}, \qquad B_{\mathrm{a},2} = \sigma_{\mathrm{t}}\left(\frac{\partial}{\partial \dot{\boldsymbol{x}}_{\mathrm{a,vol}}}\left(\frac{dJ^{-1}}{dt_{\mathrm{a}}}\right)\boldsymbol{u}_{\mathrm{a},0} + \frac{\partial \boldsymbol{R}_{\mathrm{a}}}{\partial \dot{\boldsymbol{x}}_{\mathrm{a,vol}}}\right)K_{\mathrm{m}}T_{\mathrm{d}}.$$

C. Monolithic Aeroelastic Model

We wish to couple the linear structural and aerodynamic models into a single monolithic aeroelastic system. Introducing the notation,

$$\frac{d\boldsymbol{u}_{\mathrm{s}}}{dt_{\mathrm{s}}} = \dot{\boldsymbol{u}}_{\mathrm{s}}, \tag{13}$$

we write equations (5), (12), and (13) into a complete set of aeroelastic equations,

$$\begin{bmatrix} I & 0 & 0 \\ 0 & I & 0 \\ 0 & 0 & E_{\mathrm{a}} \end{bmatrix}\frac{d}{dt_{\mathrm{s}}}\begin{bmatrix} \dot{\boldsymbol{u}}_{\mathrm{s}} \\ \boldsymbol{u}_{\mathrm{s}} \\ \boldsymbol{u}_{\mathrm{a}} \end{bmatrix} = \begin{bmatrix} 0 & A_{\mathrm{s}} & C_{\mathrm{s}} \\ I & 0 & 0 \\ B_{\mathrm{a},2} & B_{\mathrm{a},1} & A_{\mathrm{a}} \end{bmatrix}\begin{bmatrix} \dot{\boldsymbol{u}}_{\mathrm{s}} \\ \boldsymbol{u}_{\mathrm{s}} \\ \boldsymbol{u}_{\mathrm{a}} \end{bmatrix}, \tag{14}$$

where I is the identity matrix. In a more convenient form, we write this as

$$\mathbb{M}\frac{d\boldsymbol{u}}{dt_{\mathrm{s}}} = \mathbb{A}\boldsymbol{u}, \tag{15}$$

where $\boldsymbol{u}^T = \left[\dot{\boldsymbol{u}}_{\mathrm{s}}^T \ \boldsymbol{u}_{\mathrm{s}}^T \ \boldsymbol{u}_{\mathrm{a}}^T\right]$.

Analogous to the "p-method" used in flutter analysis, we expand the states into simple exponential functions in time as follows,

$$\boldsymbol{u} = \boldsymbol{v}\exp\left(\lambda t_{\mathrm{s}}\right). \tag{16}$$

This leads to the following generalized eigenvalue problem to determine the stability of the system:

$$\left(\mathbb{A} - \lambda\mathbb{M}\right)\boldsymbol{v} = \boldsymbol{0}. \tag{17}$$

We refer to equation (17) as the high-dimensional eigenproblem, and we denote any eigenvalue λ and (right) eigenvector $\boldsymbol{v}$ which satisfies (17) as a *truth* eigenvalue and *truth* eigenvector.

III. Model Order Reduction

Due to the use of the linearized Euler equations, the aeroelastic model (15) is of very high dimension and thus remains impractical for fast dynamic aeroelastic analysis. If instead of using the high-dimensional aerodynamic model (12) we approximate the behavior of the aerodynamics with a ROM, the aeroelastic eigenproblem becomes tractable. This section presents an overview of the application of projection-based model order reduction to the aerodynamic model used in this work. The approach used to form the reduced basis is discussed in Section V below.

To begin, assume we possess a set of n_{a} reduced basis vectors stored column-wise in the reduced basis $\Phi = \{\boldsymbol{\phi}_1, \boldsymbol{\phi}_2, ..., \boldsymbol{\phi}_{n_{\mathrm{a}}}\}$. In projecting equation (12) onto the reduced basis, one approximates the aerodynamic solution in the reduced space [39]:

$$\boldsymbol{u}_{\mathrm{a}} \approx \Phi \tilde{\boldsymbol{u}}_{\mathrm{a}}, \tag{18}$$

where $\tilde{\boldsymbol{u}}_{\mathrm{a}} \in \mathbb{R}^{n_{\mathrm{a}}}$ is a vector of modal coefficients. Inserting this approximation into the high-dimensional aerodynamic model (12), we obtain the residual,

$$\boldsymbol{r}_{\mathrm{ROM}} = E_{\mathrm{a}} \Phi \frac{d\tilde{\boldsymbol{u}}_{\mathrm{a}}}{dt_{\mathrm{s}}} - A_{\mathrm{a}} \Phi \tilde{\boldsymbol{u}}_{\mathrm{a}} - B_{\mathrm{a},1} \boldsymbol{u}_{\mathrm{s}} - B_{\mathrm{a},2} \dot{\boldsymbol{u}}_{\mathrm{s}}. \tag{19}$$

Enforcing the Galerkin condition, which states that the residual is orthogonal to the reduced space, leads to:

$$\Phi^T W \boldsymbol{r}_{\mathrm{ROM}} = \boldsymbol{0}, \tag{20}$$

where W is a matrix which approximates a continuous inner-product in Euclidean space. The resulting aerodynamic ROM is,

$$\Phi^T W E_{\mathrm{a}} \Phi \frac{d\tilde{\boldsymbol{u}}_{\mathrm{a}}}{dt_{\mathrm{s}}} = \Phi^T W A_{\mathrm{a}} \Phi \tilde{\boldsymbol{u}}_{\mathrm{a}} + \Phi^T W \left(B_{\mathrm{a},1} \boldsymbol{u}_{\mathrm{s}} + B_{\mathrm{a},2} \dot{\boldsymbol{u}}_{\mathrm{s}} \right). \tag{21}$$

To differentiate this aerodynamic ROM from that used for the error estimator, we denote equation (21) as the *primal* aerodynamic ROM.

Coupling the primal aerodynamic ROM to equations (5) and (13) forms the (primal) aeroelastic ROM,

$$\begin{bmatrix} I & 0 & 0 \\ 0 & I & 0 \\ 0 & 0 & \Phi^T W E_{\mathrm{a}} \Phi \end{bmatrix} \frac{d}{dt_{\mathrm{s}}} \begin{bmatrix} \dot{\boldsymbol{u}}_{\mathrm{s}} \\ \boldsymbol{u}_{\mathrm{s}} \\ \tilde{\boldsymbol{u}}_{\mathrm{a}} \end{bmatrix} = \begin{bmatrix} 0 & A_{\mathrm{s}} & C_{\mathrm{s}} \Phi \\ I & 0 & 0 \\ \Phi^T W B_{\mathrm{a},2} & \Phi^T W B_{\mathrm{a},1} & \Phi^T W A_{\mathrm{a}} \Phi \end{bmatrix} \begin{bmatrix} \dot{\boldsymbol{u}}_{\mathrm{s}} \\ \boldsymbol{u}_{\mathrm{s}} \\ \tilde{\boldsymbol{u}}_{\mathrm{a}} \end{bmatrix}, \tag{22}$$

As before, we write this in a more convenient form,

$$\tilde{\mathbb{M}} \frac{d\tilde{\boldsymbol{u}}}{dt_{\mathrm{s}}} = \tilde{\mathbb{A}} \tilde{\boldsymbol{u}}, \tag{23}$$

where $\tilde{\boldsymbol{u}}^T = \left[\dot{\boldsymbol{u}}_{\mathrm{s}}^T \; \boldsymbol{u}_{\mathrm{s}}^T \; \tilde{\boldsymbol{u}}_{\mathrm{a}}^T \right]$. One can immediately see that the matrices $\Phi^T W A_{\mathrm{a}} \Phi$ and $\Phi^T W E_{\mathrm{a}} \Phi$ are now of order n_{a}, which is typically orders of magnitude smaller than the number of degrees of freedom in the high-dimensional aerodynamic model. Assuming $\tilde{\boldsymbol{u}} = \tilde{\boldsymbol{v}} \exp\left(\tilde{\lambda} t_{\mathrm{s}}\right)$, the stability of the aeroelastic system can now be determined by the tractable eigenproblem,

$$\left(\tilde{\mathbb{A}} - \tilde{\lambda} \tilde{\mathbb{M}} \right) \tilde{\boldsymbol{v}} = \boldsymbol{0}. \tag{24}$$

In general, $\tilde{\lambda} \neq \lambda$ due to the approximation of the right eigenvector in the reduced space,

$$\boldsymbol{v} \approx \tilde{\Phi} \tilde{\boldsymbol{v}}, \tag{25}$$

with

$$\tilde{\Phi} = \begin{bmatrix} I & 0 & 0 \\ 0 & I & 0 \\ 0 & 0 & \Phi \end{bmatrix}.$$

IV. Error Estimation

The stability of the aeroelastic system is determined by the eigenvalues of the high-dimensional eigenproblem (17). In order to ensure that the aeroelastic ROM provides sufficiently accurate results relative to the high-dimensional model, we wish to estimate the error between the eigenvalues obtained from the reduced eigenproblem (24) and the corresponding truth eigenvalues. If the estimated error exceeds a user-prescribed tolerance, then the aerodynamic ROM can be trained to produce a more accurate eigenvalue. The following section presents the error estimator used in this work. The estimator is based on the work of Heuveline and Rannacher [35], who presented a DWR-based error estimator for eigenvalue problems. An overview of the approach is presented in this section; the reader is referred to Bangerth and Rannacher [40] for details of the derivation.

A. Dual-Weighted Residual-Based Error Estimation

To begin, we present the primal and dual problems of interest. The primal problem is the high-dimensional right eigenvalue problem from equation (17), rewritten here for convenience, with an extra normalization condition on the eigenvector,

$$\mathbb{A}\boldsymbol{v} = \lambda \mathbb{M}\boldsymbol{v}, \qquad \boldsymbol{v}^H \mathbb{M}\boldsymbol{v} = 1, \tag{26}$$

where a superscript ^{H} denotes the conjugate transpose. For flutter analysis, we are specifically interested in the eigenvalue; thus we define the output functional as:

$$J(\mu, \boldsymbol{w}) = \mu \boldsymbol{w}^H \mathbb{M}\boldsymbol{w}. \tag{27}$$

Due to the normalization condition, this output functional provides the eigenvalue: $J(\lambda, \boldsymbol{v}) = \lambda \boldsymbol{v}^H \mathbb{M}\boldsymbol{v} = \lambda$. For this output functional, the dual solution is obtained from the high-dimensional left eigenproblem with an added normalization condition:

$$(\boldsymbol{v}^{\mathrm{du}})^H \mathbb{A} = \lambda (\boldsymbol{v}^{\mathrm{du}})^H \mathbb{M}, \qquad (\boldsymbol{v}^{\mathrm{du}})^H \mathbb{M}\boldsymbol{v} = 1, \tag{28}$$

where $\boldsymbol{v}^{\mathrm{du}}$ is the truth left eigenvector. For further details see [40].

Now, assume we have solved the reduced (primal) eigenproblem (24) for an approximate right eigenpair $\left(\tilde{\lambda}, \tilde{\boldsymbol{v}}\right)$. Introducing this approximate eigenpair into the high-dimensional right eigenproblem (26), we obtain the following residual:

$$\boldsymbol{r} = \left(\mathbb{A} - \tilde{\lambda}\mathbb{M}\right) \tilde{\boldsymbol{\Phi}} \tilde{\boldsymbol{v}}. \tag{29}$$

Given the truth left eigenvector $\boldsymbol{v}^{\mathrm{du}}$, the error in the solution is given by the equation,

$$\lambda - \tilde{\lambda} = (\boldsymbol{v}^{\mathrm{du}})^H W \boldsymbol{r} + \mathcal{R}^{(2)}, \tag{30}$$

where $\mathcal{R}^{(2)}$ is a second-order remainder term, and, as before, W approximates an inner product [40].

Obtaining the error through equation (30) (with the remainder term neglected) remains impractical because we require the truth left eigenvector $\boldsymbol{v}^{\mathrm{du}}$ from the high-dimensional left eigenproblem (28). To reduce computational cost, it would be ideal to approximate the left eigenvector using a ROM. Importantly, the primal aeroelastic ROM (22) cannot be used because the Galerkin condition states that the residual (29) is orthogonal to the subspace spanned by the primal reduced basis. Instead, in this work we obtain an approximate left eigenvector with a second ROM, denoted as the dual ROM.

B. Dual ROM and Error Estimator

To obtain the dual aeroelastic system, we transpose the state and mass matrices from the primal high-dimensional aeroelastic model (14), giving

$$\begin{bmatrix} I & 0 & 0 \\ 0 & I & 0 \\ 0 & 0 & E_{\mathrm{a}} \end{bmatrix} \frac{d}{dt_{\mathrm{s}}} \begin{bmatrix} \dot{\boldsymbol{u}}_{\mathrm{s}}^{\mathrm{du}} \\ \boldsymbol{u}_{\mathrm{s}}^{\mathrm{du}} \\ \boldsymbol{u}_{\mathrm{a}}^{\mathrm{du}} \end{bmatrix} = \begin{bmatrix} 0 & I & B_{\mathrm{a},2}^T \\ A_{\mathrm{s}} & 0 & B_{\mathrm{a},1}^T \\ C_{\mathrm{s}}^T & 0 & A_{\mathrm{a}}^T \end{bmatrix} \begin{bmatrix} \dot{\boldsymbol{u}}_{\mathrm{s}}^{\mathrm{du}} \\ \boldsymbol{u}_{\mathrm{s}}^{\mathrm{du}} \\ \boldsymbol{u}_{\mathrm{a}}^{\mathrm{du}} \end{bmatrix}. \tag{31}$$

Note that all matrices are real and that the matrices A_{s} and E_{a} are symmetric and thus do not require a transpose. The dual aerodynamic model is then,

$$E_{\mathrm{a}} \frac{d\boldsymbol{u}_{\mathrm{a}}^{\mathrm{du}}}{dt_{\mathrm{s}}} = A_{\mathrm{a}}^T \boldsymbol{u}_{\mathrm{a}}^{\mathrm{du}} + C_{\mathrm{s}}^T \dot{\boldsymbol{u}}_{\mathrm{s}}^{\mathrm{du}}. \tag{32}$$

As for the primal aerodynamic ROM, we approximate the dual aerodynamic solution in a reduced space spanned by the reduced basis Φ^{du}:

$$\boldsymbol{u}_{\mathrm{a}}^{\mathrm{du}} \approx \Phi^{\mathrm{du}} \tilde{\boldsymbol{u}}_{\mathrm{a}}^{\mathrm{du}}, \tag{33}$$

where $\tilde{\boldsymbol{u}}_{\mathrm{a}}^{\mathrm{du}}$ is a vector of modal coefficients. From this approximation, we obtain the residual,

$$\boldsymbol{r}_{\mathrm{ROM}}^{\mathrm{du}} = E_{\mathrm{a}} \Phi^{\mathrm{du}} \frac{d\tilde{\boldsymbol{u}}_{\mathrm{a}}^{\mathrm{du}}}{dt_{\mathrm{s}}} - A_{\mathrm{a}}^{T} \Phi^{\mathrm{du}} \tilde{\boldsymbol{u}}_{\mathrm{a}}^{\mathrm{du}} - C_{\mathrm{s}}^{T} \dot{\boldsymbol{u}}_{\mathrm{s}}^{\mathrm{du}}. \tag{34}$$

Enforcing the Galerkin condition $\left(\Phi^{\mathrm{du}}\right)^{T} W \boldsymbol{r}_{\mathrm{ROM}}^{\mathrm{du}} = \mathbf{0}$ leads to the dual aerodynamic ROM,

$$\left(\Phi^{\mathrm{du}}\right)^{T} W E_{\mathrm{a}} \Phi^{\mathrm{du}} \frac{d\tilde{\boldsymbol{u}}_{\mathrm{a}}^{\mathrm{du}}}{dt_{\mathrm{s}}} = \left(\Phi^{\mathrm{du}}\right)^{T} W A_{\mathrm{a}}^{T} \Phi^{\mathrm{du}} \tilde{\boldsymbol{u}}_{\mathrm{a}}^{\mathrm{du}} + \left(\Phi^{\mathrm{du}}\right)^{T} W C_{\mathrm{s}}^{T} \dot{\boldsymbol{u}}_{\mathrm{s}}^{\mathrm{du}}. \tag{35}$$

Armed with this dual aerodynamic ROM, we can form the dual aeroelastic ROM,

$$\begin{bmatrix} I & 0 & 0 \\ 0 & I & 0 \\ 0 & 0 & \left(\Phi^{\mathrm{du}}\right)^{T} W E_{\mathrm{a}} \Phi^{\mathrm{du}} \end{bmatrix} \frac{d}{dt_{\mathrm{s}}} \begin{bmatrix} \dot{\boldsymbol{u}}_{\mathrm{s}}^{\mathrm{du}} \\ \boldsymbol{u}_{\mathrm{s}}^{\mathrm{du}} \\ \tilde{\boldsymbol{u}}_{\mathrm{a}}^{\mathrm{du}} \end{bmatrix} = \begin{bmatrix} 0 & I & B_{\mathrm{a},2}^{T} \Phi^{\mathrm{du}} \\ A_{\mathrm{s}} & 0 & B_{\mathrm{a},1}^{T} \Phi^{\mathrm{du}} \\ \left(\Phi^{\mathrm{du}}\right)^{T} W C_{\mathrm{s}}^{T} & 0 & \left(\Phi^{\mathrm{du}}\right)^{T} W A_{\mathrm{a}}^{T} \Phi^{\mathrm{du}} \end{bmatrix} \begin{bmatrix} \dot{\boldsymbol{u}}_{\mathrm{s}}^{\mathrm{du}} \\ \boldsymbol{u}_{\mathrm{s}}^{\mathrm{du}} \\ \tilde{\boldsymbol{u}}_{\mathrm{a}}^{\mathrm{du}} \end{bmatrix}. \tag{36}$$

In a more convenient form, we write this as

$$\tilde{\mathbb{M}}^{\mathrm{du}} \frac{d\tilde{\boldsymbol{u}}^{\mathrm{du}}}{dt_{\mathrm{s}}} = \tilde{\mathbb{A}}^{\mathrm{du}} \tilde{\boldsymbol{u}}^{\mathrm{du}}. \tag{37}$$

This directly leads to the reduced dual generalized eigenproblem,

$$\left(\tilde{\mathbb{A}}^{\mathrm{du}} - \tilde{\lambda}^{\mathrm{du}} \tilde{\mathbb{M}}^{\mathrm{du}}\right) \tilde{\boldsymbol{v}}^{\mathrm{du}} = \mathbf{0}, \tag{38}$$

where $\tilde{\boldsymbol{v}}^{\mathrm{du}}$ is a reduced approximation of the truth left eigenvector $\boldsymbol{v}^{\mathrm{du}}$ such that

$$\boldsymbol{v}^{\mathrm{du}} \approx \tilde{\boldsymbol{\Phi}}^{\mathrm{du}} \tilde{\boldsymbol{v}}^{\mathrm{du}}, \tag{39}$$

with

$$\tilde{\boldsymbol{\Phi}}^{\mathrm{du}} = \begin{bmatrix} I & 0 & 0 \\ 0 & I & 0 \\ 0 & 0 & \Phi^{\mathrm{du}} \end{bmatrix}. \tag{40}$$

Introducing the left eigenvector approximation (39) into equation (30), and neglecting the remainder term, we obtain the error estimator η used in this work:

$$\lambda - \tilde{\lambda} \approx \eta \equiv \left(\tilde{\boldsymbol{\Phi}}^{\mathrm{du}} \tilde{\boldsymbol{v}}^{\mathrm{du}}\right)^{H} W \boldsymbol{r}. \tag{41}$$

V. Reduced Basis Training

In this section, we define our approach to constructing an aeroelastic ROM capable of predicting aeroelastic eigenvalues to a user-prescribed accuracy. But first, we define the parameter on which our aeroelastic ROMs depend. Aerodynamic parameters including the Mach number and angle of attack are held fix during our analyses. Similarly, structural parameters such as the structural mass and Young's modulus are also held fix. The parameter for the aeroelastic ROMs is the variable which affects the coupling between both the aerodynamic and structural models. For our purposes, the aeroelastic parameter can be either the dynamic pressure q_∞ or the speed index $V = \frac{V_\infty}{b\omega_\alpha \mu}$, where V_∞ is the freestream speed, b is the root semichord, ω_α is the uncoupled first torsional frequency, and μ is the mass ratio. The results presented in Section VII use aeroelastic systems formulated using the speed index. But to keep the approach more general, we denote both q_∞ and V as the "aeroelastic parameter" and use the placeholder μ.

The error estimator (41) allows us to approximate the error in any eigenvalue obtained from the reduced aeroelastic eigenproblem (24). However, not all eigenvalues obtained from the aeroelastic ROM are important for flutter analysis. Certain eigenmodes in the aeroelastic system are closely associated to the modes of the structural model, and it is one of these eigenmodes that will become unstable. At low aeroelastic parameter values, these are easily determined because

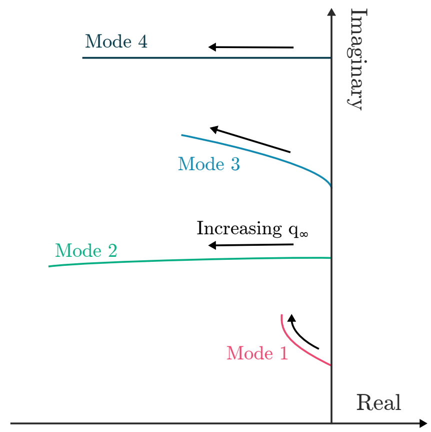

Fig. 1 Example of an aeroelastic root locus plot for increasing dynamic pressure, showing only important aeroelastic modes.

each eigenvalue has an imaginary part near the natural frequency of its associated structural mode. As the aeroelastic parameter is increased, the eigenvalues change in value. Figure 1 demonstrates an example root locus for increasing dynamic pressure for an aeroelastic system with four structural modes.

Based on this knowledge, we wish to create a reduced basis that spans the subspace of the eigenvectors of these important eigenmodes for a range of aeroelastic parameter values. In this pursuit, we require three algorithmic elements: a means of constructing an initial reduced basis, a robust eigenvalue tracking algorithm, and a means of approximating truth eigenvectors. The eigenvalue tracking algorithm is required to know which eigenvalues are relevant for flutter analysis and necessitate error estimation. A means of approximating truth eigenvectors is required in order to train the reduced basis to obtain better approximations of aeroelastic eigenvalues. In this section, we present our approach to each of the aforementioned elements.

A. Reduced Basis Initialization

When initializing the primal and dual reduced bases, Φ and Φ^{du}, the goal is not to create aeroelastic ROMs which can accurately predict the aeroelastic eigenvalues. Rather, the goal is to create primal and dual ROMs which can estimate the error in the eigenvalues with sufficient accuracy. In this work, the initial primal and dual reduced bases are constructed from solutions of the primal and dual high-dimensional aerodynamic models in the frequency-domain. To obtain these equations, the aerodynamic and structural vectors are assumed to be harmonic,

$$\boldsymbol{u}_{\mathrm{a}}(t) = \sum_j \bar{\boldsymbol{u}}_{\mathrm{a},j} e^{i\omega t}, \qquad \boldsymbol{u}_{\mathrm{s}}(t) = \sum_j \bar{\boldsymbol{u}}_{\mathrm{s},j} e^{i\omega t}, \tag{42}$$

where $\bar{\boldsymbol{u}}_{\mathrm{a},j}$ and $\bar{\boldsymbol{u}}_{\mathrm{s},j}$ are the aerodynamic and structural Fourier coefficients, respectively. Inserting these expressions into the high-dimensional linearized aerodynamic model (12), we obtain the governing primal aerodynamic equations in the frequency-domain,

$$(i\omega E_{\mathrm{a}} - A_{\mathrm{a}})\, \bar{\boldsymbol{u}}_{\mathrm{a},j} = \left(B_{\mathrm{a},1} + i\omega B_{\mathrm{a},2}\right) \bar{\boldsymbol{u}}_{\mathrm{s},j}. \tag{43}$$

Using the same approach, we can convert the high-dimensional dual aerodynamic model (32) to the frequency-domain,

$$\left(i\omega E_{\mathrm{a}} - A_{\mathrm{a}}^T\right) \bar{\boldsymbol{u}}^{\mathrm{du}}_{\mathrm{a},j} = i\omega C_{\mathrm{a}}^T \bar{\boldsymbol{u}}^{\mathrm{du}}_{\mathrm{s},j}. \tag{44}$$

To obtain initial snapshots for the reduced bases, equations (43) and (44) are solved for several aeroelastic parameter values. At each aeroelastic parameter value, these equations are solved for ω equal to the natural frequencies of the structure. At each natural frequency, the corresponding generalized velocity and displacement are set to unity and the inverse frequency, respectively, in the input vectors $\bar{\boldsymbol{u}}_{\mathrm{s},j}$ and $\bar{\boldsymbol{u}}^{\mathrm{du}}_{\mathrm{s},j}$. Note that changing the aeroelastic parameter value results in changes to the system matrices in equations (43) and (44) due to different time and force scaling factors σ_{t} and σ_{f}.

We have found that solving equations (43) and (44) for five aeroelastic parameter values produces initial ROMs with good error estimation capability. Moreover, the equations are solved only to a relative tolerance of 10^{-1} to obtain the initial snapshots. Once all of the snapshots of $\bar{\boldsymbol{u}}_{\mathrm{a},j}$ and $\bar{\boldsymbol{u}}^{\mathrm{du}}_{\mathrm{a},j}$ have been obtained, they are orthogonalized using the modified Gram-Schmidt procedure and used to create the initial reduced bases Φ and Φ^{du}. Note that the real and imaginary parts of the snapshots are included as separate vectors in Φ and Φ^{du} to produce only real valued reduced bases.

B. Eigenvalue Tracking

Once the aeroelastic ROMs have been initialized, the reduced eigenproblem (24) can be used to approximate aeroelastic eigenvalues. At aeroelastic parameter values near zero, the eigenvalues relevant for flutter analysis are those with an imaginary part near a natural frequency of the structure. As the aeroelastic parameter value is increased, the values of these eigenvalues change, which leads to the need for tracking. Assume we have an approximate eigenvalue $\tilde{\lambda}^{(n-1)}$ known to be important for flutter analysis at the aeroelastic parameter increment $n-1$. At increment n, after solving the eigenproblem (24), we have a number of approximate eigenvalues $\tilde{\lambda}_i^{(n)}$ for $i = 1, 2, \ldots$, and we wish to know which eigenvalue $\tilde{\lambda}_i^{(n)}$ is associated to the known eigenvalue $\tilde{\lambda}^{(n-1)}$. Several algorithms have been proposed for this purpose [41, 42]. In this work, we use a mixture of three metrics to track the eigenvalues.

The first tracking metric is based on the use of the error estimator (41). At increment n, we have the approximate eigenvalues $\tilde{\lambda}_i^{(n)}$, and approximate right and left eigenvectors, $\tilde{\boldsymbol{v}}_i^{(n)}$ and $\tilde{\boldsymbol{v}}_i^{\mathrm{du}(n)}$, respectively. Assuming the eigenvectors vary smoothly with changing aeroelastic parameter value, we can use the left eigenvector at the previous increment associated to the known eigenvalue $\tilde{\lambda}^{(n-1)}$ to estimate the error in the new i^{th} approximate eigenvalue,

$$\sigma_i^{\mathrm{err}} \equiv \left(\boldsymbol{w}_{\mathbb{A}}^H - \tilde{\lambda}_i^{(n)} \boldsymbol{w}_{\mathbb{M}}^H\right) \tilde{\boldsymbol{v}}_i^{(n)}, \tag{45}$$

where

$$\boldsymbol{w}_{\mathbb{A}}^H = \left(\tilde{\Phi}^{\mathrm{du}} \tilde{\boldsymbol{v}}^{\mathrm{du}(n-1)}\right)^H W \mathbb{A}^{(n)} \tilde{\Phi}, \qquad \boldsymbol{w}_{\mathbb{M}}^H = \left(\tilde{\Phi}^{\mathrm{du}} \tilde{\boldsymbol{v}}^{\mathrm{du}(n-1)}\right)^H W \mathbb{M}^{(n)} \tilde{\Phi},$$

and $\tilde{\boldsymbol{v}}^{\mathrm{du}(n-1)}$ is the approximate left eigenvector for the known eigenvalue $\tilde{\lambda}^{(n-1)}$. One can see that if we replace the vector $\tilde{\boldsymbol{v}}^{\mathrm{du}(n-1)}$ with $\tilde{\boldsymbol{v}}^{\mathrm{du}(n)}$ in equation (45) above, we regain the standard error estimator from (41). Thus the only difference between the error estimators (45) and (41) is the use of a left eigenvector at a previous aeroelastic parameter value. The vectors $\boldsymbol{w}_{\mathbb{A}}^H$ and $\boldsymbol{w}_{\mathbb{M}}^H$ need only be computed once at each aeroelastic parameter increment, and therefore the term σ_j^{err} is efficient to compute for all approximate eigenvalues.

The second metric is the magnitude of the difference between the eigenvalues,

$$\sigma_i^{\mathrm{diff}} \equiv \left|\tilde{\lambda}^{(n-1)} - \tilde{\lambda}_i^{(n)}\right|. \tag{46}$$

The third metric is the eigenvector correlation-based method of van Zyl [41]. It can be compactly expressed as

$$\sigma_i^{\mathrm{corr}} \equiv \frac{\left|\left(\tilde{\boldsymbol{v}}^{(n-1)}\right)^H \tilde{\boldsymbol{v}}_i^{(n)}\right|}{\left\|\tilde{\boldsymbol{v}}^{(n-1)}\right\|_2 \left\|\tilde{\boldsymbol{v}}_i^{(n)}\right\|_2},$$

where $\tilde{\boldsymbol{v}}^{(n-1)}$ and $\tilde{\boldsymbol{v}}_i^{(n)}$ are the reduced right eigenvectors associated to $\tilde{\lambda}^{(n-1)}$ and $\tilde{\lambda}_i^{(n)}$, respectively.

Once computed, all of the metrics σ_i are normalized so that their values over all indices i sum to one. Subsequently, the three metrics are aggregated into a logarithmic opinion pool,

$$p_i = \left(\sigma_i^{\mathrm{err}}\right)^{w_1} \left(\sigma_i^{\mathrm{diff}}\right)^{w_2} \left(\sigma_i^{\mathrm{corr}}\right)^{w_3}, \tag{47}$$

where the weights w_1, w_2, and w_3 sum to one. The eigenvalue $\tilde{\lambda}_i^{(n)}$ with the largest value of p_i is assumed to be associated to $\tilde{\lambda}^{(n-1)}$. However, the largest value of p_i must be at least 50% higher than second largest value, otherwise the tracking is flagged as a failure and the aeroelastic parameter step is halved. For the results obtained in this paper, the following weight values were found to provide reliable eigenvalue tracking:

$$w_1 = 0.5, \qquad w_2 = 0.4, \qquad w_3 = 0.1.$$

C. Reduced Basis Updates using Approximate Eigenvectors

Using the eigenvalue tracking method outlined above, we can determine which approximate eigenvalues from the aeroelastic ROMs are relevant for flutter analysis. Furthermore, using the error estimator (41), we can estimate the error in these approximate eigenvalues. If the error of an eigenvalue is above a user-prescribed tolerance, then an approximate truth eigenvalue and approximate right and left truth eigenvectors are computed for the high-dimensional eigenvalue problem (17). The new truth eigenvectors are then added to primal and dual reduced bases. By repeating this process for various aeroelastic parameter values, we can create aeroelastic ROMs capable of approximating the aeroelastic eigenvalues over a range of aeroelastic parameter values to a user-prescribed tolerance.

In this work, a two-sided refined Jacobi-Davidson method [30–32] is used to solve the high-dimensional eigenproblem (17). This algorithm allows for both the left and right eigenvectors to be obtained simultaneously for the eigenvalue nearest a user-specified target. We choose the approximate eigenvalue $\tilde{\lambda}^{(n)}$ as the target. To minimize computation costs, we have developed a new stopping criterion for the method. At each iteration k, the two-sided Jacobi-Davidson method provides a new approximate (truth) right eigenvector $\boldsymbol{v}^{(k)}$ and left eigenvector $\boldsymbol{v}^{\mathrm{du}(k)}$. The Rayleigh quotient of the right eigenvector approximates the truth eigenvalue, and is computed as

$$\theta^{(k)} = \frac{\left(\boldsymbol{v}^{(k)}\right)^H \mathbb{A}\boldsymbol{v}^{(k)}}{\left(\boldsymbol{v}^{(k)}\right)^H \mathbb{M}\boldsymbol{v}^{(k)}}, \tag{48}$$

Using the approximate truth left eigenvector $\boldsymbol{v}^{\mathrm{du}(k)}$, the error in this Rayleigh quotient can be estimated as,

$$\lambda - \theta^{(k)} \approx \left(\boldsymbol{v}^{\mathrm{du}(k)}\right)^H W\boldsymbol{r}_\theta, \tag{49}$$

where $\boldsymbol{r}_\theta$ is the residual associated to the Rayleigh quotient,

$$\boldsymbol{r}_\theta = \mathbb{A}\boldsymbol{v}^{(k)} - \theta^{(k)}\mathbb{M}\boldsymbol{v}^{(k)}.$$

Thus, the two-sided Jacobi-Davidson method is run until the error estimate (49) is below the user-set tolerance for the Rayleigh quotient error.

Once the Jacobi-Davidson algorithm has sufficiently converged, it provides approximate truth right and left eigenvectors $\boldsymbol{v}$ and $\boldsymbol{v}^{\mathrm{du}}$, respectively. Note that the eigenvectors are composed of structural and aerodynamic parts: $\boldsymbol{v}^T = \left[\dot{\boldsymbol{v}}_\mathrm{s}^T,\ \boldsymbol{v}_\mathrm{s}^T,\ \boldsymbol{v}_\mathrm{a}^T\right]$. To update the primal and dual aerodynamic ROMs, the aerodynamic part of the eigenvalues are added to the existing reduced bases. The right eigenvectors are added to the primal reduced basis Φ, while the left eigenvectors are added to the dual reduced basis Φ^{du}. The real and imaginary parts are included separately in order to keep the reduced bases, and hence the reduced matrices, real valued,

$$\Phi = \{\boldsymbol{\phi}_1, \boldsymbol{\phi}_2, \ldots, \mathrm{Real}\{\boldsymbol{v}_\mathrm{a}\}, \mathrm{Imag}\{\boldsymbol{v}_\mathrm{a}\}\},$$
$$\Phi^{\mathrm{du}} = \left\{\boldsymbol{\phi}_1^{\mathrm{du}}, \boldsymbol{\phi}_2^{\mathrm{du}}, \ldots, \mathrm{Real}\{\boldsymbol{v}_\mathrm{a}^{\mathrm{du}}\}, \mathrm{Imag}\{\boldsymbol{v}_\mathrm{a}^{\mathrm{du}}\}\right\}.$$

To ensure proper conditioning of the reduced matrices, the new vectors are orthogonalized with respect to all other basis vectors using the modified Gram-Schmidt procedure.

VI. ROM-Based Flutter Prediction

With the reduced basis training procedure presented Section V, we can create an aeroelastic ROM which can model the behavior of the aeroelastic HDM to a user-prescribed accuracy. In this section, we present our approach to solve for the flutter point.

As a first step, the ROM training procedure is applied to create an aeroelastic ROM which can approximate aeroelastic eigenvalues. The training procedure is stopped once one of these aeroelastic eigenvalues crosses the imaginary axis, indicating the onset of flutter in the system. This process is graphically shown in Figure 2 as a flow chart. Once an unstable eigenvalue is found in the system, the calculation of the flutter point begins. The exact aeroelastic parameter value at which flutter occurs for the aeroelastic ROM is obtained using the Hopf point calculation method of Griewank and Reddien [43]. However, because the aeroelastic ROM is made to approximate the linearized aeroelastic equations, it cannot be used to approximate the solution of the nonlinear equations which govern the static aeroelastic deflection. For the test cases presented in this paper, the geometries are symmetric and the angles of attack are kept at zero degrees; therefore no static aeroelastic deflections are present in the system. This eliminates the need to solve the nonlinear static

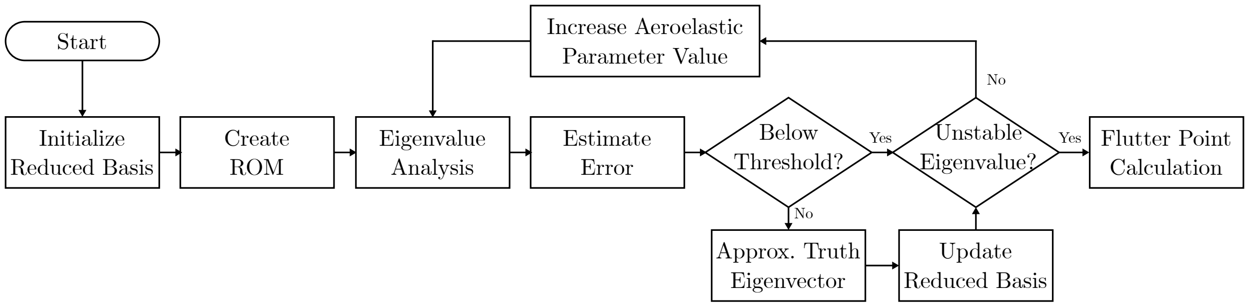

Fig. 2 ROM-based flutter prediction methodology.

aeroelastic equations for changing aeroelastic parameter values. If a geometry is nonsymmetric or the angle of attack is non-zero, then an iterative approach can be used where the Hopf point is computed for a fixed static solution, followed by an update to the static solution to reflect the new Hopf point parameter value.

The Hopf point is computed for the aeroelastic ROM, therefore the computations are fast. However, the aeroelastic parameter value at which the aeroelastic ROM flutters may be different from that of the high-dimensional aeroelastic system. Therefore, we wish to approximate the error in the flutter point from the ROM. We denote the aeroelastic parameter value at which the high-dimensional system flutters as μ^{flutter}, and that at which the aeroelastic ROM flutters as $\tilde{\mu}^{\text{flutter}}$. Remember that the aeroelastic parameter μ is a placeholder for either the dynamic pressure q_∞ or the speed index V. Assuming μ^{flutter} can be expressed as a function of the real part of the aeroelastic eigenvalue, we expand it into a Taylor series about $\tilde{\mu}^{\text{flutter}}$,

$$\mu^{\text{flutter}} = \tilde{\mu}^{\text{flutter}} + \frac{d\mu}{d\lambda_r}\left(0 - \lambda_r\right) + O\left(\lambda_r^2\right), \tag{50}$$

where λ_r is the real part of the truth eigenvalue at the aeroelastic parameter value $\tilde{\mu}^{\text{flutter}}$. The real part of the approximate eigenvalue from the aeroelastic ROM $\tilde{\lambda}_r$ is zero at $\tilde{\mu}^{\text{flutter}}$; we introduce it in equation (50) to eventually retrieve the eigenvalue error estimator. Hence, an error estimate for the flutter point can be obtained as,

$$\left|\mu^{\text{flutter}} - \tilde{\mu}^{\text{flutter}}\right| \approx \left|\frac{d\lambda_r}{d\mu}\right|^{-1} \left|\lambda_r - \tilde{\lambda}_r\right|. \tag{51}$$

The difference in the real part of the truth and approximate eigenvalues is estimated using,

$$\left|\lambda_r - \tilde{\lambda}_r\right| \approx \left|\text{Real}\{\eta\}\right|, \tag{52}$$

where η is the error estimator from (41). The derivative in equation (51) is inverted to simplify its computation. We approximate this derivative using the approximate right and left eigenvectors from the primal and dual ROMs such that

$$\frac{d\lambda_r}{d\mu} \approx \text{Real}\left\{\left(\tilde{\mathbf{\Phi}}^{\text{du}}\tilde{\boldsymbol{v}}^{\text{du}}\right)^{H}\left(\frac{d\mathbb{A}}{d\mu} - \tilde{\lambda}\frac{d\mathbb{M}}{d\mu}\right)\tilde{\mathbf{\Phi}}\tilde{\boldsymbol{v}}\right\}. \tag{53}$$

Ultimately, we can combine equations (51), (52), and (53) to obtain an error estimator for the flutter point,

$$\left|\mu^{\text{flutter}} - \tilde{\mu}^{\text{flutter}}\right| \approx \eta_{\text{f}} \equiv \left|\text{Real}\left\{\left(\tilde{\mathbf{\Phi}}^{\text{du}}\tilde{\boldsymbol{v}}^{\text{du}}\right)^{H}\left(\frac{d\mathbb{A}}{d\mu} - \tilde{\lambda}\frac{d\mathbb{M}}{d\mu}\right)\tilde{\mathbf{\Phi}}\tilde{\boldsymbol{v}}\right\}\right|^{-1} \left|\text{Real}\{\eta\}\right|. \tag{54}$$

Using this error estimator, we can determine if the approximated flutter point $\tilde{\mu}^{\text{flutter}}$ is sufficiently accurate. If it is not, then the aeroelastic primal and dual ROMs are updated using eigenvectors obtained at $\tilde{\mu}^{\text{flutter}}$ using the Jacobi-Davidson approach outlined in Section V.C. The Hopf point is then recalculated for the updated aeroelastic ROM, and the flutter point error is once again computed. This process is repeated until the error estimator η_{f} is below the user-specified tolerance.

VII. Results

This section presents results for the dynamic aeroelastic analysis of a two degree of freedom structural model and for the AGARD 445.6 wing test case obtained using the methodology outlined above. The aeroelastic models use the

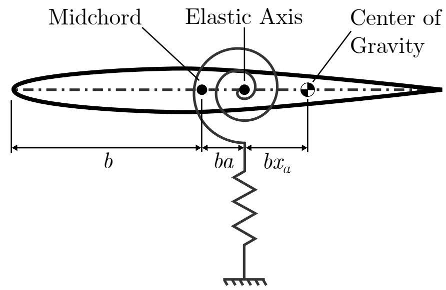

Fig. 3 Two degree of freedom airfoil structure capable of pitching and plunging.

speed index V as the aeroelastic parameter. For analysis purposes, the truth eigenvalues are obtained by reducing the norm of the residual of the high-dimensional right eigenproblem (17) below a tolerance of 10^{-14}. The truth eigenvalues are used to compute the exact errors, which are used to determine the effectiveness of the error estimator.

A. Two Degree of Freedom Aeroelastic Test Case

To test the accuracy and efficiency of the proposed approach, the two degree of freedom airfoil structure shown in Figure 3 is used. The structure is supported by a torsional and a linear spring and is capable of both pitching and plunging. Aeroelastic results are presented for Case A of Isogai [44]. Dynamic aeroelastic analyses are performed about a steady-state angle of attack of 0°. All simulations pertaining to this model are performed on the NACA 64A010 airfoil with a structured O-mesh. The mesh consists of 38,000 nodes around the airfoil subdivided into 32 blocks. All results are obtained using 32 Intel "Skylake" cores at 2.4 GHz.

1. Aeroelastic Root Locus

The aeroelastic root locus for this test case was obtained for a Mach number of 0.85 and a series of speed indices between 0.01 and 1.0. A user-prescribed tolerance of

$$|\eta| \leq 10^{-3}$$

was used for all aeroelastic eigenvalues. Figure 4 displays the root locus obtained from the aeroelastic ROM after initializing the reduced bases, but prior to training the ROM using eigenvectors from the Jacobi-Davidson algorithm. Figure 5 shows the converged root locus once the training the procedure is complete and all eigenvalue error estimates are below the user-prescribed tolerance. On the right of these figures, we present the root locus of the aeroelastic eigenvalues. On the left, we show the nondimensional damping and frequencies for each mode in the system, these are the real and imaginary parts of the associated eigenvalues, respectively. Moreover, both the error estimate and exact error are plotted for all speed indices. Exact errors for mode 2 at speed indices 0.65 and 0.7 are omitted from the results because the norm of the high-dimensional eigenproblem residual could not be brought to a tolerance of 10^{-14}.

The results in Figure 4 are presented to demonstrate the behavior of the error estimator at the beginning of the ROM training process. From the figure, we can see that the error estimator slightly under predicts the exact error, but generally captures the order of magnitude of the exact error quite well. Moreover, we see that the initial aeroelastic ROM does not predict any instability in the system as no eigenvalues are seen crossing the imaginary axis in Figure 4. One can expect that this may change as the ROM is trained to reduce the error in eigenvalues.

Results in Figure 5 show the behavior of the aeroelastic system once the training is completed and all estimated eigenvalue errors are below the user-specified tolerance of 10^{-3}. We can see that the behavior of the aeroelastic eigenvalues has changed significantly from that presented in Figure 4. One now observes an instability in Mode 1 above a speed index of approximately 0.5. This indicates the onset of flutter in the system, which is analyzed further in subsequent results. Moreover, Mode 2 now demonstrates higher damping, but also shows early signs of reversal at speed index 1.0. For these final results, we see that the error estimator agrees very well with the exact error at speed indices above 0.2. Below this, the error estimator tends to slightly underpredict the error, just as it did for the initial results from Figure 4. This is because the error estimates at these speed indices are below the user-prescribed tolerance, and therefore the ROM is not updated at these low speed indices. In general, when comparing the error estimate to the exact error, we observe very good agreement for the converged results in Figure 5. The time breakdown to obtain the full root

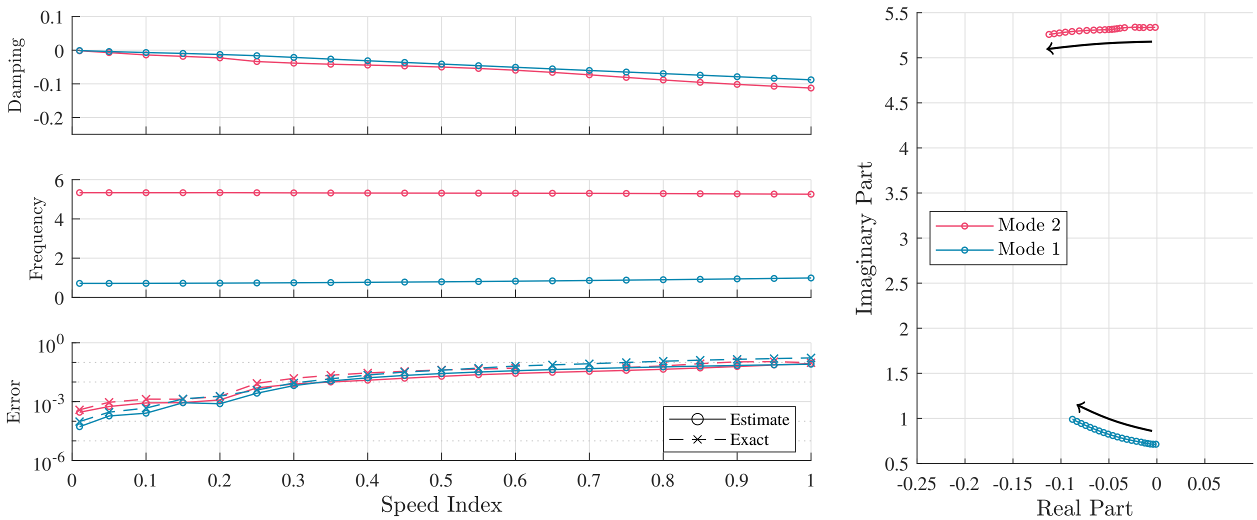

Fig. 4 Aeroelastic mode damping, frequency, and error (left), and root locus plot (right) for the two degree of freedom model at Mach 0.85 obtained immediately after the reduced basis initialization.

locus shown in Figure 5 was 16% for the steady flow solve, 7% for the reduced basis initialization, and 77% for the reduced basis training. This translates to an equivalent time of 6.3 nonlinear steady flow solves to obtain the root locus.

2. Flutter Boundary

To obtain the flutter boundary for the two degree of freedom system, aeroelastic ROMs were constructed for a series of Mach numbers between 0.75 and 0.875. For the ROM training procedure, a tolerance of

$$\left|\frac{\mathrm{Real}\{\eta\}}{\mathrm{Real}\{\tilde{\lambda}\}}\right| \leq 10^{-1}$$

was used. In other words, a relative error tolerance was placed on the real part of the eigenvalues. A step size of 0.05 in speed index was used for the computation of the root locus. The ROM training persisted until one of the eigenvalues in the system crossed the imaginary axis, at which point the Hopf point calculation was used to obtain the exact flutter point. A relative flutter speed index error tolerance of

$$\frac{\eta_{\mathrm{f}}}{\tilde{V}_{\mathrm{f}}} \leq 0.005$$

was used as a stopping criterion, where η_{f} is the error estimator for the flutter point given in equation (54), and $\tilde{V}_{\mathrm{f}}$ is the flutter speed index of the aeroelastic ROM.

Figure 6 shows the flutter boundary obtained using our approach, along with a pie chart showing the time breakdown for each part of the analysis. One can see that the results are in good agreement with those obtained by Alonso and Jameson [45] and Sanchez *et al*. [46], both of whom used the Euler equations. The resurgence of stability at Mach 0.875 can be obtained from the aeroelastic ROM for the current approach, but is omitted for our purposes. From the time breakdown shown in Figure 6, it is clear that the bulk of the time (71%) is required for the reduced basis training procedure. The majority of this time is spent obtaining approximate truth left and right eigenvectors with the Jacobi-Davidson algorithm. This time analysis demonstrates that with the methodology presented, the time required to obtain a flutter point is approximately 5 times the time required for one steady nonlinear flow solve. This time is less than that required to obtain the root locus shown in Figure 5 because of the relaxed tolerance on the eigenvalues and because the root locus in Figure 5 extends beyond the flutter point.

B. AGARD 445.6 Test Case

We present results obtained for the dynamic aeroelastic analysis of the AGARD 445.6 test case. Flutter predictions for the wing were originally obtained with wind tunnel testing performed by Yates [47]. The structural model provided

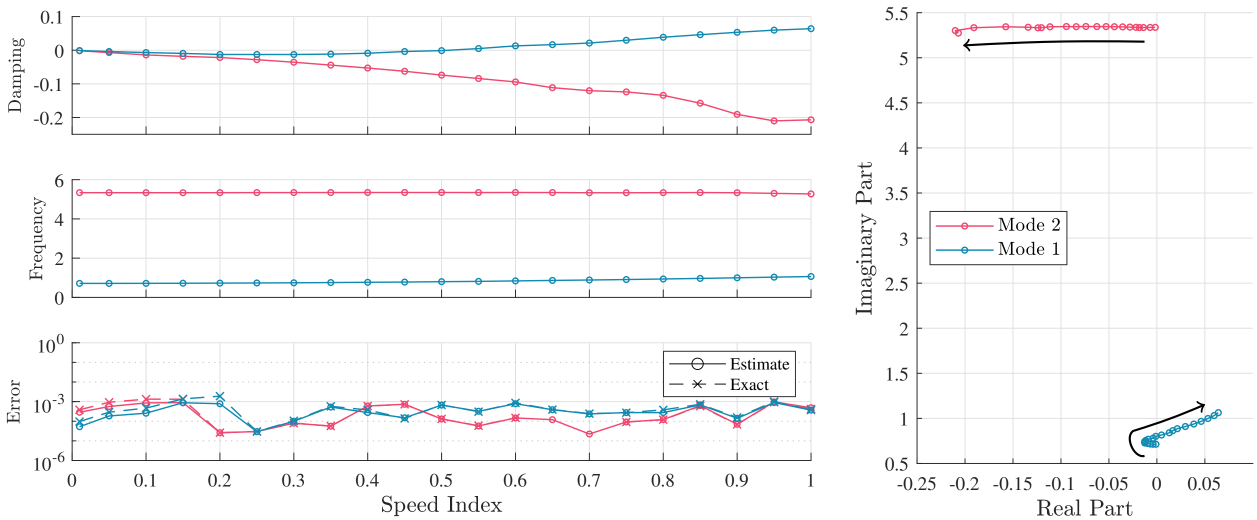

Fig. 5 Aeroelastic mode damping, frequency, and error (left), and root locus plot (right) for the two degree of freedom model at Mach 0.85 obtained after the complete ROM training procedure.

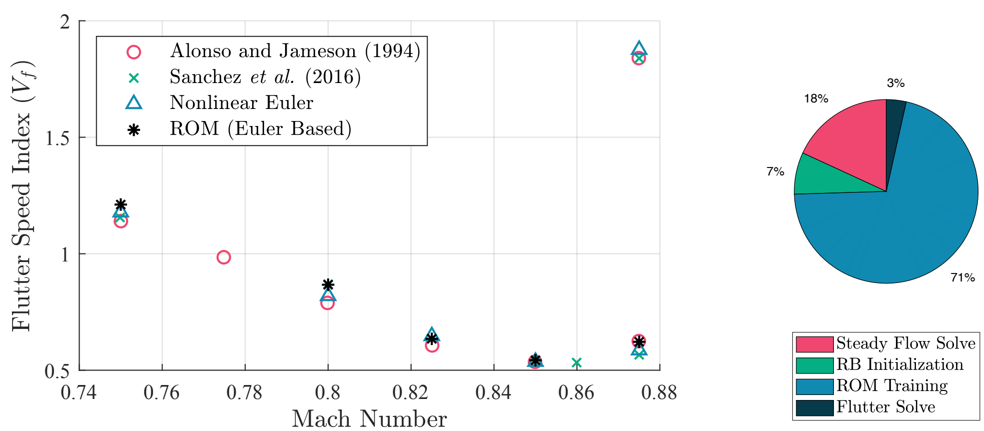

Fig. 6 Flutter boundary (left) and time breakdown (right) for the two degree of freedom model.

by Yates [47] is composed of four natural frequencies and mode shapes, the latter shown in Figure 7. Simulations are performed on the AGARD 445.6 wing geometry using a structured H-C mesh with 1,987,392 nodes subdivided into 160 blocks. All results are obtained using 160 Intel "Skylake" cores at 2.4 GHz.

1. Aeroelastic Root Locus

Here we present the aeroelastic root locus of the AGARD 445.6 wing model obtained for a Mach number of 0.901. To obtain this root locus, a relative eigenvalue tolerance of

$$\frac{|\eta|}{|\tilde{\lambda}|} \leq 10^{-3}$$

was used. Figure 8 shows the damping, frequency, and estimated errors for the four modes of the AGARD wing at various values of speed indices, along with the root locus of the eigenvalues. From this figure, we observe that all eigenvalues are below the user-specified tolerance. The instability in the system for this case is due to the first mode, which crosses the imaginary axis at a speed index of approximately 0.35.

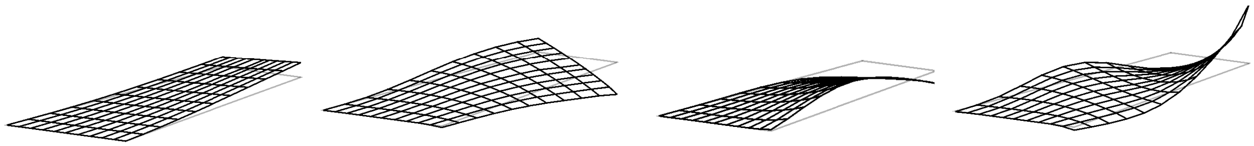

(a) Mode 1 **(b) Mode 2** **(c) Mode 3** **(d) Mode 4**

Fig. 7 First four mode shapes of the AGARD 445.6 wing structure.

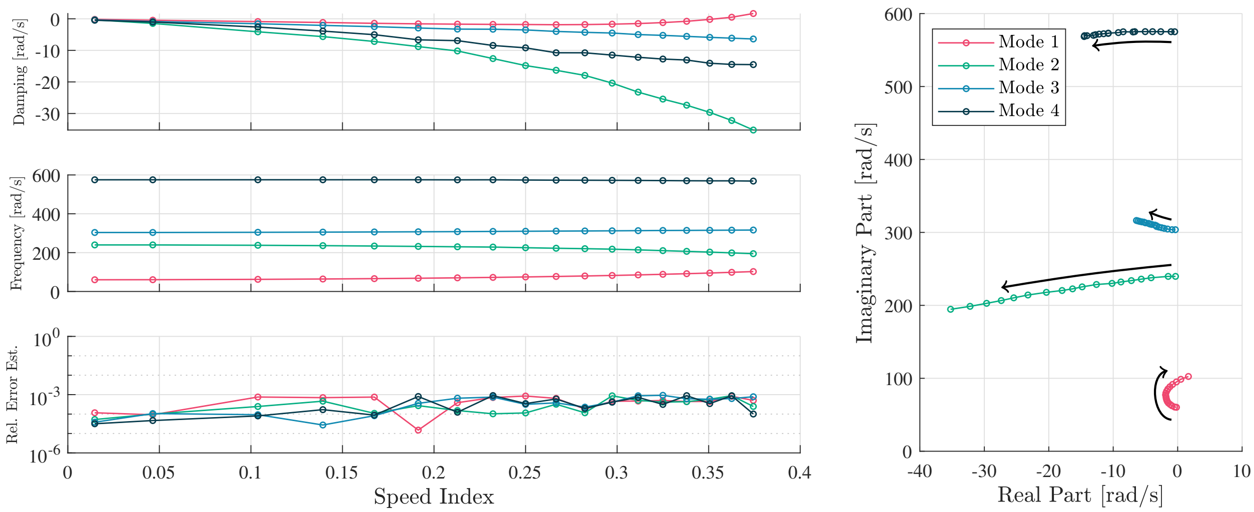

Fig. 8 Aeroelastic mode damping, frequency, and relative estimated error (left), and root locus plot (right) for the AGARD 445.6 wing at Mach 0.901.

2. Flutter Boundary

To obtain the flutter boundary for the AGARD 445.6 model, aeroelastic ROMs were constructed for each Mach number of interest. As for the two degree of freedom case, a tolerance of

$$\left|\frac{\mathrm{Real}\{\eta\}}{\mathrm{Real}\{\tilde{\lambda}\}}\right| \leq 10^{-1}$$

was used for the eigenvalues. Moreover, a step size of 0.05 in speed index was used for the computation of the root locus, and a relative flutter speed index error tolerance of

$$\frac{\eta_{\mathrm{f}}}{\tilde{V}_{\mathrm{f}}} \leq 0.005$$

was used as a stopping criterion.

Figure 9 shows the flutter boundary obtained using our approach, along with a pie chart showing the time breakdown for each part of the analysis. The flutter boundary obtained experimentally by Yates [47] and computationally by Silva *et al*. [19] are also included in this figure. As expected, flutter predictions at the lower Mach numbers match well with those obtained experimentally by Yates [47]. At high Mach numbers, namely 0.960, 1.072, and 1.141, it has been shown that the Euler equations do not accurately predict the flutter boundary due the absence of viscosity [48].

To further analyze the behavior of the system, Figure 10 shows the root locus plots obtained for each Mach number for the AGARD 445.6 wing. There are several things to note from these plots. First, the root locus at Mach 0.499 shows some jagged behavior in the migration of the eigenvalues, especially evident for the changes in mode 2. This behavior is due to the loose tolerance set on the eigenvalue errors. Second, at the Mach numbers 1.072 and 1.141, the onset of flutter is due to an instability in the third aeroelastic mode. It has been shown by Silva *et al*. [19] that this instability is an artifact resulting from the use of the Euler equations.

From the time analysis in Figure 9, we can see that computing each point on the flutter boundary took an average equivalent time of approximately 4 steady nonlinear Euler flow solves. In this case, the majority of the time (57%) was taken to compute the initial reduced bases.

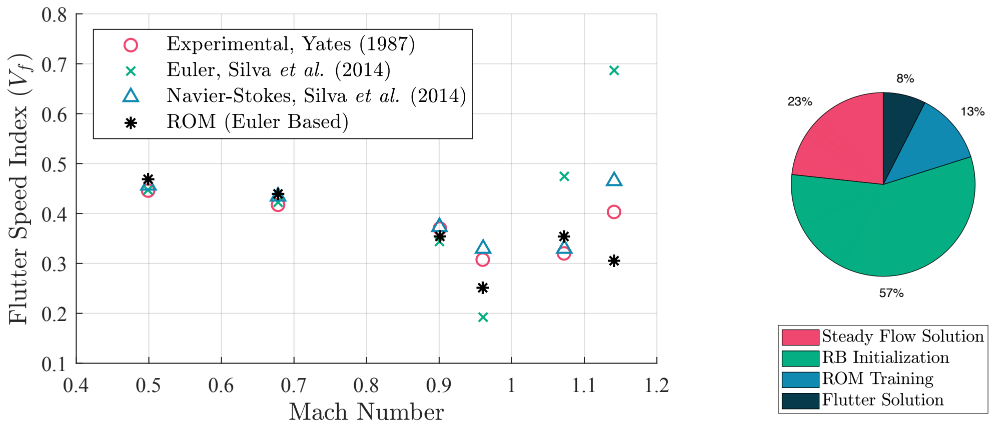

Fig. 9 Flutter boundary (left) and time breakdown (right) for the AGARD 445.6 wing model.

VIII. Conclusions

This paper presents a methodology for dynamic aeroelastic analysis using a projection-based model order reduction approach with error estimation capable of ensuring that the error relative to the high-dimensional model is within a user-defined tolerance. The DWR method has been used to provide an estimate of the error of the eigenvalues obtained from the reduced aeroelastic eigenproblem. Moreover, we have presented a procedure for training the reduced basis which incorporates the use of the error estimator. Results show that this methodology is effective for obtaining the root locus and the flutter boundary of a two degree of freedom structural model and for the AGARD 445.6 wing test case for a series of speed indices. The error estimator is shown to compare well with the exact error for the two degree of freedom case. This work presents a means by which dynamic aeroelastic analysis can be performed such that a prescribed level of accuracy is obtained relative to the high-dimensional aeroelastic model. For the test cases presented in this work, the cost of computing the flutter point at a given Mach number is equivalent to the cost of approximately 4 to 5 steady nonlinear flow evaluations of the high-dimensional Euler equations.

Future work includes using the linearized RANS equations as the aerodynamic model to provide better flutter predictions at high Mach numbers. Additionally, the aeroelastic eigenvalues obtained from this algorithm can be used as a flutter constraint for aerodynamic shape optimization. This can be accomplished by placing a constraint on the real part of the eigenvalues. Significant computational savings may be obtained by using the reduced basis constructed at a previous optimization iteration to form the initial aeroelastic ROM at the current iteration.

Acknowledgements

This research was enabled in part by the financial support provided by Bombardier, the Government of Ontario, the Natural Sciences and Research Council of Canada, and the University of Toronto. Computational resources were provided by SciNet HPC Consortium, a part of Compute Canada. The authors are extremely grateful for the input and support provided by Masayuki Yano.

References

[1] Reist, T. A., Zingg, D. W., Rakowitz, M., Potter, G., and Banerjee, S., "Multifidelity Optimization of Hybrid Wing–Body Aircraft with Stability and Control Requirements," *Journal of Aircraft*, Vol. 56, No. 2, 2019, pp. 442–456. doi:10.2514/1.C034703.

[2] Bendiksen, O. O., "Review of Unsteady Transonic Aerodynamics: Theory and Applications," *Progress in Aerospace Sciences*, Vol. 47, No. 2, 2011, pp. 135–167. doi:10.1016/j.paerosci.2010.07.001.

[3] Henshaw, M., Badcock, K., Vio, G., Allen, C., Chamberlain, J., Kaynes, I., Dimitriadis, G., Cooper, J., Woodgate, M., Rampurawala, A., Jones, D., Fenwick, C., Gaitonde, A., Taylor, N., Amor, D., Eccles, T., and Denley, C., "Non-Linear Aeroelastic Prediction for Aircraft Applications," *Progress in Aerospace Sciences*, Vol. 43, No. 4, 2007, pp. 65–137. doi:10.1016/j.paerosci.2007.05.002.

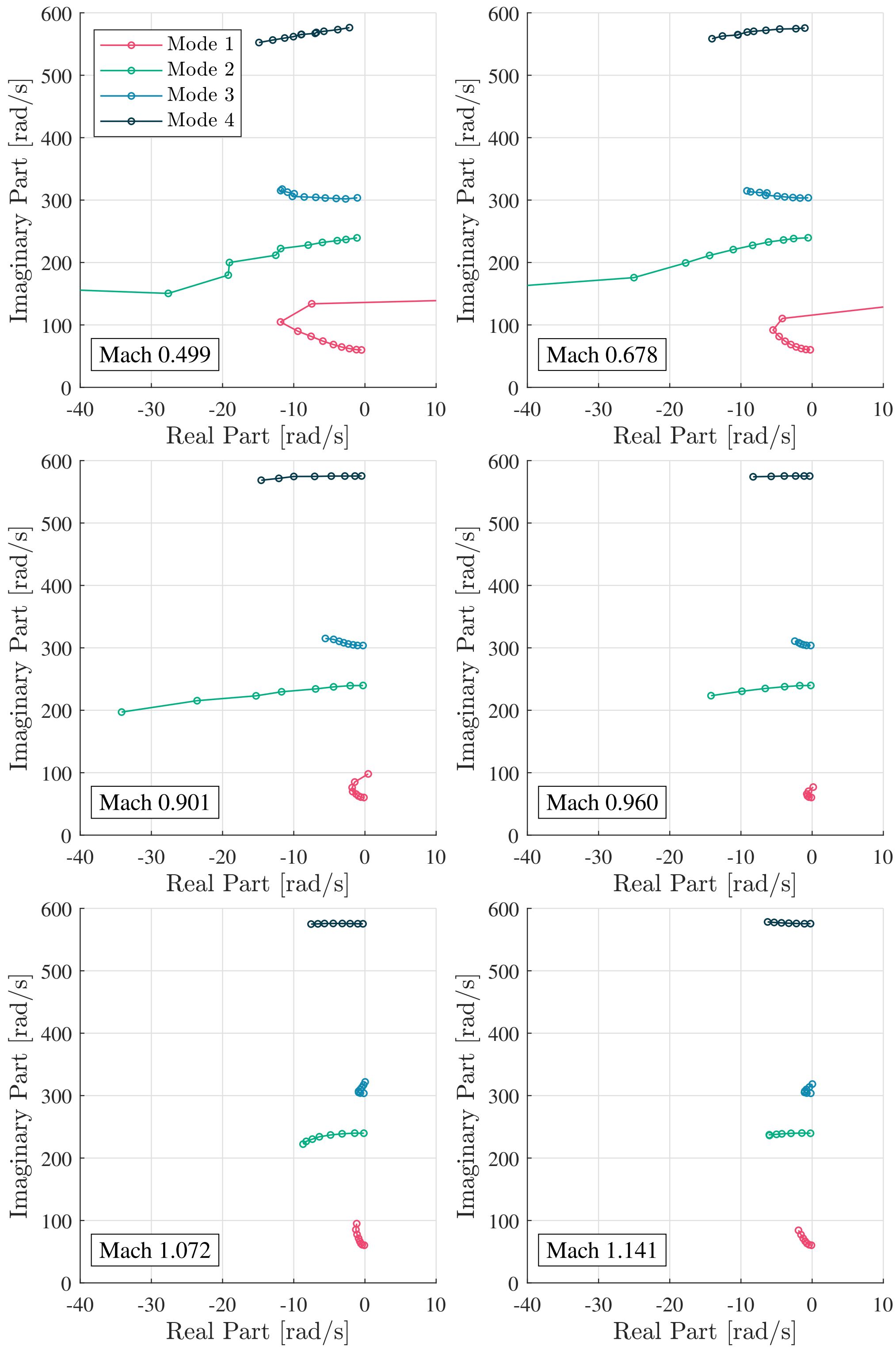

Fig. 10 Aeroelastic root locus plots for the AGARD 445.6 wing test case at various Mach numbers.

[4] Beran, P., and Lutton, M., "Hopf Bifurcation in Viscous Flows about Airfoils at Low Speeds," *22nd Fluid Dynamics, Plasma Dynamics and Lasers Conference*, Honolulu, Hawaii, 1991. doi:10.2514/6.1991-1807.

[5] Morton, S. A., and Beran, P. S., "Hopf-Bifurcation Analysis of Airfoil Flutter at Transonic Speeds," *Journal of Aircraft*, Vol. 36, No. 2, 1999, pp. 421–429. doi:10.2514/2.2447.

[6] Woodgate, M., and Badcock, K., "Fast Prediction of Transonic Aeroelastic Stability and Limit Cycles," *AIAA Journal*, Vol. 45, No. 6, 2007, pp. 1370–1381.

[7] Jacobson, K., Stanford, B., Wood, S., and Anderson, W. K., "Flutter Analysis with Stabilized Finite Elements based on the Linearized Frequency-domain Approach," *AIAA SciTech 2020 Forum*, 2020. doi:10.2514/6.2020-0403.

[8] He, S., Jonsson, E., Mader, C. A., and Martins, J. R. R. A., "Coupled Newton–Krylov Time-Spectral Solver for Flutter and Limit Cycle Oscillation Prediction," *AIAA Journal*, Vol. 59, No. 6, 2021, pp. 2214–2232. doi:10.2514/1.J059224.

[9] Opgenoord, M. M. J., Drela, M., and Willcox, K. E., "Influence of Transonic Flutter on the Conceptual Design of Next-Generation Transport Aircraft," *AIAA Journal*, Vol. 57, No. 5, 2019, pp. 1973–1987. doi:10.2514/1.J057302.

[10] Hall, K. C., Thomas, J. P., and Dowell, E. H., "Proper Orthogonal Decomposition Technique for Transonic Unsteady Aerodynamic Flows," *AIAA Journal*, Vol. 38, No. 10, 2000, pp. 1853–1862. doi:10.2514/2.867.

[11] Thomas, J. P., Dowell, E. H., and Hall, K. C., "Three-Dimensional Transonic Aeroelasticity Using Proper Orthogonal Decomposition-Based Reduced-Order Models," *Journal of Aircraft*, Vol. 40, No. 3, 2003, pp. 544–551. doi:10.2514/2.3128.

[12] Beran, P. S., Lucia, D. J., and Pettit, C. L., "Reduced-Order Modelling of Limit-Cycle Oscillation for Aeroelastic Systems," *Journal of Fluids and Structures*, Vol. 19, No. 5, 2004, pp. 575–590. doi:10.1016/j.jfluidstructs.2004.04.002.

[13] Anttonen, J. S., King, P. I., and Beran, P. S., "Applications of Multi-POD to a Pitching and Plunging Airfoil," *Mathematical and Computer Modelling*, Vol. 42, No. 3, 2005, pp. 245–259. doi:10.1016/j.mcm.2005.06.003.

[14] Lieu, T., Farhat, C., and Lesoinne, M., "Reduced-Order Fluid/Structure Modeling of a Complete Aircraft Configuration," *Computer Methods in Applied Mechanics and Engineering*, Vol. 195, No. 41, 2006, pp. 5730–5742. doi:10.1016/j.cma.2005.08.026.

[15] Lieu, T., and Farhat, C., "Adaptation of Aeroelastic Reduced-Order Models and Application to An F-16 Configuration," *AIAA Journal*, Vol. 45, No. 6, 2007, pp. 1244–1257. doi:10.2514/1.24512.

[16] Kim, T., Hong, M., Bhatia, K. G., and SenGupta, G., "Aeroelastic Model Reduction for Affordable Computational Fluid Dynamics-based Flutter Analysis," *AIAA Journal*, Vol. 43, No. 12, 2005, pp. 2487–2495. doi:10.2514/1.11246.

[17] Kim, T., "System Identification for Coupled Fluid-Structure: Aerodynamics is Aeroelasticity Minus Structure," *AIAA Journal*, Vol. 49, No. 3, 2011, pp. 503–512. doi:10.2514/1.J050245.

[18] Zhang, W., Wang, B., Ye, Z., and Quan, J., "Efficient Method for Limit Cycle Flutter Analysis Based on Nonlinear Aerodynamic Reduced-Order Models," *AIAA Journal*, Vol. 50, No. 5, 2012, pp. 1019–1028. doi:10.2514/1.J050581.

[19] Silva, W. A., Chwalowski, P., and Perry III, B., "Evaluation of Linear, Inviscid, Viscous, and Reduced-order Modelling Aeroelastic Solutions of the AGARD 445.6 Wing using Root Locus Analysis," *International Journal of Computational Fluid Dynamics*, Vol. 28, No. 3-4, 2014, pp. 122–139. doi:10.1080/10618562.2014.922179.

[20] Silva, W., "AEROM: NASA's Unsteady Aerodynamic and Aeroelastic Reduced-Order Modeling Software," *Aerospace*, Vol. 5, No. 2, 2018, pp. 41–58. doi:10.3390/aerospace5020041.

[21] Badcock, K. J., Timme, S., Marques, S., Khodaparast, H., Prandina, M., Mottershead, J., Swift, A., Da Ronch, A., and Woodgate, M., "Transonic Aeroelastic Simulation for Instability Searches and Uncertainty Analysis," *Progress in Aerospace Sciences*, Vol. 47, No. 5, 2011, pp. 392–423. doi:10.1016/j.paerosci.2011.05.002.

[22] Amsallem, D., Tezaur, R., and Farhat, C., "Real-Time Solution of Linear Computational Problems Using Databases of Parametric Reduced-Order Models with Arbitrary Underlying Meshes," *Journal of Computational Physics*, Vol. 326, 2016, pp. 373–397. doi:10.1016/j.jcp.2016.08.025.

[23] Bekemeyer, P., and Timme, S., "Flexible Aircraft Gust Encounter Simulation Using Subspace Projection Model Reduction," *Aerospace Science and Technology*, Vol. 86, 2019, pp. 805–817. doi:10.1016/j.ast.2019.02.011.

[24] Kou, J., and Zhang, W., "A Hybrid Reduced-Order Framework for Complex Aeroelastic Simulations," *Aerospace Science and Technology*, Vol. 84, 2019, pp. 880 – 894. doi:10.1016/j.ast.2018.11.014.

[25] Waite, J., Stanford, B., Bartels, R. E., and Silva, W. A., "Reduced Order Modeling for Transonic Aeroservoelastic Control Law Development," *AIAA SciTech 2019 Forum*, San Diego, California, 2019. doi:10.2514/6.2019-1022.

[26] Argaman, M., and Raveh, D. E., "Multioutput Autoregressive Aeroelastic System Identification and Flutter Prediction," *Journal of Aircraft*, Vol. 56, No. 1, 2019, pp. 30–42. doi:10.2514/1.C034789.

[27] Lowe, B. M., and Zingg, D. W., "Efficient Flutter Prediction Using Reduced-Order Modeling," *AIAA Journal*, published online, March 2021. doi:10.2514/1.J060006.

[28] Juang, J.-N., and Pappa, R. S., "An Eigensystem Realization Algorithm for Modal Parameter Identification and Model Reduction," *Journal of Guidance, Control, and Dynamics*, Vol. 8, No. 5, 1985, pp. 620–627. doi:10.2514/3.20031.

[29] Becker, R., and Rannacher, R., "An Optimal Control Approach to A Posteriori Error Estimation in Finite Element Methods," *Acta Numerica*, Vol. 10, No. 1, 2001, pp. 1–102. doi:10.1017/S0962492901000010.

[30] Sleijpen, G. L., and Van der Vorst, H. A., "A Jacobi–Davidson Iteration Method for Linear Eigenvalue Problems," *SIAM Review*, Vol. 42, No. 2, 2000, pp. 267–293. doi:10.1137/S0036144599363084.

[31] Hochstenbach, M. E., and Sleijpen, G. L., "Two-sided and Alternating Jacobi–Davidson," *Linear Algebra and its Applications*, Vol. 358, No. 1-3, 2003, pp. 145–172. doi:10.1016/S0024-3795(01)00494-3.

[32] Feng, S., and Jia, Z., "A refined Jacobi-Davidson method and its correction equation," *Computers & Mathematics with Applications*, Vol. 49, No. 2-3, 2005, pp. 417–427.

[33] Benner, P., Hochstenbach, M. E., and Kürschner, P., "Model Order Reduction of Large-scale Dynamical Systems with Jacobi-Davidson style Eigensolvers," *2011 International Conference on Communications, Computing and Control Applications (CCCA)*, 2011, pp. 1–6. doi:10.1109/CCCA.2011.6031208.

[34] Fidkowski, K. J., and Darmofal, D. L., "Review of Output-based Error Estimation and Mesh Adaptation in Computational Fluid Dynamics," *AIAA Journal*, Vol. 49, No. 4, 2011, pp. 673–694.

[35] Heuveline, V., and Rannacher, R., "A Posteriori Error Control for Finite Element Approximations of Elliptic Eigenvalue Problems," *Advances in Computational Mathematics*, Vol. 15, No. 1-4, 2001, pp. 107–138. doi:10.1023/A:1014291224961.

[36] Rendall, T., and Allen, C., "Unified Fluid–Structure Interpolation and Mesh Motion Using Radial Basis Functions," *International Journal for Numerical Methods in Engineering*, Vol. 74, No. 10, 2008, pp. 1519–1559. doi:10.1002/nme.2219.

[37] Brown, S., "Displacement Extrapolations for CFD+CSM Aeroelastic Analysis," *38th Structures, Structural Dynamics, and Materials Conference*, Kissimmee, Florida, 1997. doi:10.2514/6.1997-1090.

[38] Thomas, P., and Lombard, C., "Geometric Conservation Law and its Application to Flow Computations on Moving Grids," *AIAA Journal*, Vol. 17, No. 10, 1979, pp. 1030–1037. doi:10.2514/3.61273.

[39] Benner, P., Gugercin, S., and Willcox, K., "A Survey of Projection-Based Model Reduction Methods for Parametric Dynamical Systems," *SIAM Review*, Vol. 57, No. 4, 2015, pp. 483–531. doi:10.1137/130932715.

[40] Bangerth, W., and Rannacher, R., *Adaptive Finite Element Methods for Differential Equations*, Birkhäuser, Basel, Switzerland, 2003. doi:10.1007/978-3-0348-7605-6.

[41] van Zyl, L. H., "Use of Eigenvectors in the Solution of the Flutter Equation," *Journal of Aircraft*, Vol. 30, No. 4, 1993, pp. 553–554. doi:10.2514/3.46380.

[42] Eldred, M., Venkayya, V., and Anderson, W., "New Mode Tracking Methods in Aeroelastic Analysis," *AIAA Journal*, Vol. 33, No. 7, 1995, pp. 1292–1299. doi:10.2514/3.12552.

[43] Griewank, A., and Reddien, G., "The Calculation of Hopf Points by a Direct Method," *IMA Journal of Numerical Analysis*, Vol. 3, No. 3, 1983, pp. 295–303. doi:10.1093/imanum/3.3.295.

[44] Isogai, K., "Numerical Study of Transonic Flutter of a Two-Dimensional Airfoil," Tech. Rep. TR-617T, National Aerospace Laboratory, July 1980.

[45] Alonso, J., and Jameson, A., "Fully-Implicit Time-Marching Aeroelastic Solutions," *32nd Aerospace Sciences Meeting and Exhibit*, Reno, Nevada, 1994. doi:10.2514/6.1994-56.

[46] Sanchez, R., Kline, H., Thomas, D., Variyar, A., Righi, M., Economon, T. D., Alonso, J. J., Palacios, R., Dimitriadis, G., and Terrapon, V., "Assessment of the Fluid-structure Interaction Capabilities for Aeronautical Applications of the Open-source Solver SU2," *Proceedings of the VII European Congress on Computational Methods in Applied Science and Engineering*, ECCOMAS, Crete Island, Greece, 2016, pp. 1498–1529. doi:10.7712/100016.1903.6597.

[47] Yates Jr, E. C., "AGARD Standard Aeroelastic Configurations for Dynamic Response. Candidate Configuration I.-Wing 445.6," Tech. Rep. N88-11202, National Aeronautics and Space Administration, 1987.

[48] Lee-Rausch, E., and Batina, J., "Calculation of AGARD Wing 445.6 Flutter Using Navier-Stokes Aerodynamics," *11th Applied Aerodynamics Conference*, Monterey, California, 1993. doi:10.2514/6.1993-3476.